J Geod (2005) 78: 660–667
DOI 10.1007/s00190-004-0432-z

ORIGINAL ARTICLE

R. Mautz · J. Ping · K. Heki · B. Schaffrin
C. Shum · L. Potts

Efficient spatial and temporal representations of global ionosphere maps over Japan using B-spline wavelets

Received: 19 January 2004 / Accepted: 4 December 2004 / Published online: 18 April 2005

Abstract Wavelet expansion has been demonstrated to be suitable for the representation of spatial functions. Here we propose the so-called B-spline wavelets to represent spatial time-series of GPS-derived global ionosphere maps (GIMs) of the vertical total electron content (TEC) from the Earth's surface to the mean altitudes of GPS satellites, over Japan. The scalar-valued B-spline wavelets can be defined in a two-dimensional, but not necessarily planar, domain. Generated by a sequence of knots, different degrees of B-splines can be implemented: degree 1 represents the Haar wavelet; degree 2, the linear B-spline wavelet, or degree 4, the cubic B-spline wavelet. A non-uniform version of these wavelets allows us to handle data on a bounded domain without any edge effects. B-splines are easily extended with great computational efficiency to domains of arbitrary dimensions, while preserving their properties. This generalization employs tensor products of B-splines, defined as linear superposition of products of univariate B-splines in different directions. The data and model may be identical at the locations of the data points if the number of wavelet coefficients is equal to the number of grid points. In addition, data compression is made efficient by eliminating the wavelet coefficients with negligible magnitudes, thereby reducing the observational noise. We applied the developed methodology to the representation of the spatial and temporal variations of GIM from an extremely dense GPS network, the GPS Earth Observation Network (GEONET) in Japan. Since the sampling of the TEC is registered regularly in time, we use a two-dimensional B-spline wavelet representation in space and a one-dimensional spline interpolation in time. Over the Japan region, the B-spline wavelet method can overcome the problem of bias for the spherical harmonic model at the boundary, caused by the non-compact support. The hierarchical decomposition not only allows an inexpensive calculation, but also separates visualisation at different levels of detail. Each level corresponds to a certain spatial frequency band, leading to a detection of structures and enhancement in the ionosphere at different resolutions.

Keywords B-spline wavelets · Ionosphere · Total electron content (TEC) · Multi-resolution representation

R. Mautz
Centre for Transport Studies, Department of Civil and Environmental Engineering, Imperial College London,
Skempton Building, London SW7 2AZ, United Kingdom
E-mail: r.mautz@imperial.ac.uk
Tel.: +44-20-7594-6037
Fax: +44-20-7594-6102

R. Mautz · B. Schaffrin · C. Shum (✉) · L. Potts
Laboratory for Space Geodesy and Remote Sensing,
The Ohio State University,
(470 Hitchcock Hall, 2070 Neil Avenue),
Columbus, OH 43210, USA
E-mail: ckshum@osu.edu

J. Ping
Shanghai Astronomical Observatory,
80 Nandan Road, Shanghai 200030, China

K. Heki
Division of Earth and Planetary Sciences, Graduate School of Science,
Hokkaido University,
Kita-ku N10 W8, Sapporo 060-0810, Japan

1 Introduction

During the last decade, wavelet expansion has become one of the principal geodetic research foci for efficient representation of spatial data. More recently, studies have been extended to four-dimensional datasets such as atmospheric observations. With the availability of new and more precise space geodetic sensors, there is a fast-growing amount of geodetic data with heterogeneous distribution and distinct accuracies to be analyzed. The powerful and flexible tool known as "wavelet series" was established in geodesy, allowing multi-resolution representations of multi-dimensional data. In this context, Freeden (1999), Salamonowicz (2001) and Schmidt (2001), among others, have exploited wavelets for various geodetic applications.

A special class of wavelets is generated by B-splines ("B" stands for basis), offering useful properties such as compact support, semi-orthogonality, symmetry, and simplicity. B-splines on a bounded interval were introduced by Chui

and Quak (1992), whereas decomposition and reconstruction algorithms are presented in Quak and Weyrich (1994). Spline-wavelets serve as one of the most popular families of interpolators: given a sampled signal, for example at integer points, the signal at any real point can easily be interpolated, preserving essential properties such as smoothness and continuity. Our approach also takes advantage of the multiresolution representation of the surface data. Furthermore, B-splines and B-spline wavelets are of compact support (zero-valued outside a bounded region), which contributes to their computational efficiency because of their limited overlap.

This paper contributes to the implementation of the two-dimensional B-spline wavelets, which are described in Sects. 2 and 3. Applications and algorithms can be found in Stollnitz et al. (1996). The mathematical background for spline functions on the sphere is described by Lyche and Schumaker (2000). Attempts to use B-spline wavelets to model geoid undulations have been made by Mautz et al. (2002) and Schaffrin et al. (2003), whereas Potts (2003) propose a representation of the ionosphere using four-dimensional spherical wavelets.

The total electron content (TEC) is the number of electrons in a column of 1 m^2 cross-sectional area along a radial trans-ionospheric path from an altitude in space to the surface of the Earth. The TEC provides a measure of the ionospheric delay that affects electromagnetic signals, including those used for navigation. These delays are frequency dependent. In the case of L-band (GPS) signals, the delay is ∼16 m (up to 100 TECU, or TEC units, 1 TECU = 10^{16} electrons/m^2). A continuously operating reference station (CORS) network of GPS receivers allows one to observe first-order ionosphere delays or TECs by combining the dual-frequency GPS L-band signals at the phase centers of each GPS antenna globally (e.g., Schaer et al. 1995) or within a regional area (Wilson et al. 1995; Ping et al. 2002, 2003).

In order to detect spatial structures of a few tens of kilometer over Japan, we use the GPS Earth Observation Network (GEONET) operated by the Geographical Survey Institute (GSI) of Japan, comprising over 1000 stations typically separated by ∼25 km (Saito et al. 1998). Using GEONET, the daily relative TEC perturbations were mapped by Saito et al. (1998), and the absolute TEC in the zenith direction corresponding to the relative TEC map can be obtained, for example, by a technique developed by Otsuka et al. (2002). Construction of a regional ionospheric model (RIM) based on spherical functions is described by Ping et al. (2002).

The global spherical harmonic basis function has two disadvantages for a bounded spherical function representation. First, with increasing order and degree of the spherical harmonic expansion, the size of the series may become very large, which inhibits efficient computation. Second, the data cut-off at boundaries introduces a bias into the harmonic model representing the data (cf. the Gibbs phenomenon). In order to efficiently represent local TEC values for a region like Japan with high spatial and temporal resolution, instead of using global basis functions, a bounded wavelet basis can overcome the problem of inefficiency.

2 Definition of B-spline spaces

2.1 Unbounded domain

The characteristic function χ for B-splines on the real axis is identical to the Haar scaling function, which can also be seen as the B-spline of degree one, denoted by $\chi = B^1$. Its definition is

$$B^1(x) := \begin{cases} 1 & \text{for } 0 \le x < 1, \\ 0 & \text{otherwise.} \end{cases} \tag{1}$$

B-splines of higher degrees $d > 1$ are defined recursively by

$$B^d(x) = \int_0^1 B^{d-1}(x-t)\mathrm{d}t \tag{2}$$

The level space of uniform B-splines, including their translated and scaled versions, reads

$$B^d_{j,k}(x) := B^d\left(2^j x - k\right) \tag{3}$$

where the degree d is a positive integer, $j \in \mathrm{Z}$ is the level of detail and $k \in \mathrm{Z}$ is the shift along the x-axis of the spline function. The spline function can be reconstructed through a sum of scaled and translated copies of itself, known as the two-scale relation:

$$B^d(x) = \sum_{k=0}^{d} p_k B^d(2x-k) \tag{4}$$

with

$$p_k = 2^{1-d}\binom{d}{k} \tag{5}$$

The constant numbers in front of the B-splines are known as the refinement coefficients (for a given degree d). Since the two-scale relation (Eq. 4) allows switching between different scales, we define

$$\phi^d(x) := B^d(x) \tag{6}$$

as scaling functions ϕ. Based on this choice, Chui and Wang (1992) introduced the compactly supported B-spline wavelets ψ of constant order d, namely

$$\psi^d(x) = 2^{-(d-1)} \sum_{s=0}^{2d-2} (-1)^s B^{2d}(s+1) \cdot \left(B^{2d}\right)^{(d)}(2x-s) \tag{7}$$

where the d-th derivative is denoted by $^{(d)}$. With $d = 1$ we get the well-known Haar function ψ^1. From Eq. (7) and the spline identity

$$\left(B^{2d}\right)^{(d)}(x) = \sum_{r=0}^{d} (-1)^r \binom{d}{r} B^d(x-r) \tag{8}$$

as well as the substitutions $k = s + r$ and $k_{\max} = 3d - 2$, the simplified form for the B-spline wavelet reads

$$\psi^d(x) = \sum_{k=0}^{3d-2} q_k B^d(2x-k) \tag{9}$$

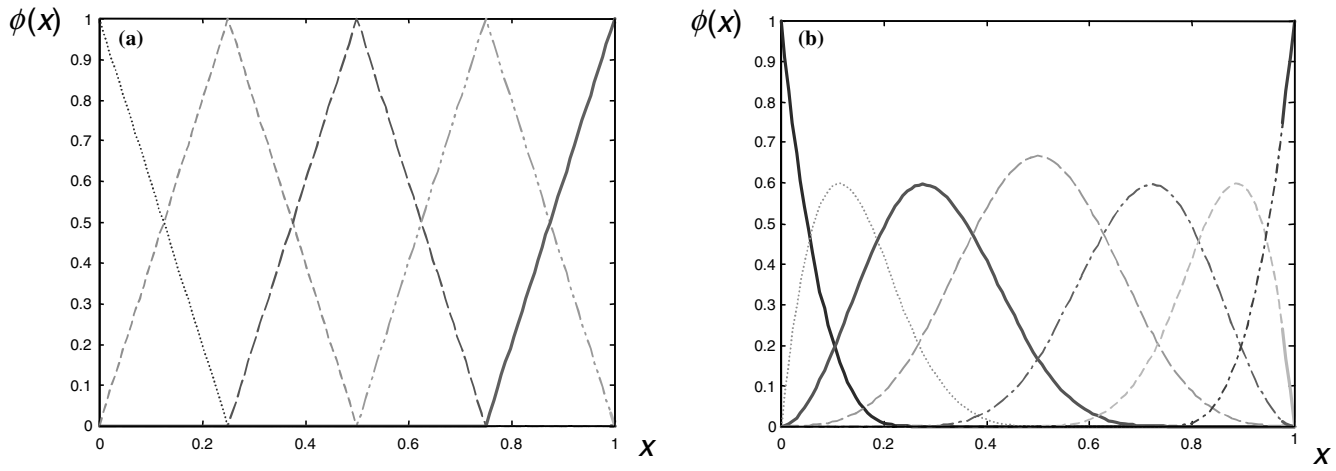

Fig. 1 **a** The five one-dimensional linear ($d = 2$) B-spline scaling functions of level $j = 2$. **b** The seven one-dimensional cubic ($d = 4$) B-spline scaling functions of level $j = 2$

where q_k are refinement coefficients for the wavelets expressed by

$$q_k = \frac{(-1)^k}{2^{n-1}} \sum_{t=0}^{d} \binom{d}{t} B^{2d}(k - t + 1) \tag{10}$$

For the unbounded domain, the refinement coefficients p_k and q_k can be stored as simple column-vectors because the scaling and wavelet functions are invariant to the shift along the parametric axes of the observational domain.

2.2 Bounded domain

The motivation for the bounded domain version is to avoid edge effects at the boundaries. In this case, the first $d - 1$ B-spline functions next to the boundaries differ from each other. Thus, it is necessary to create a space of scaling functions, in the following, denoted by ϕ. Considering the piecewise constant characteristic function $\chi = \phi^1$ for the spline of degree one

$$\phi_k^1(x) := \begin{cases} 1 & \text{if } x_k \le x < x_{k+1}, \\ 0 & \text{otherwise,} \end{cases} \tag{11}$$

where x is the function variable and x_k are members of the knot sequence

$$(x_0, \ldots x_{2^j+2d-2}) = \tfrac{1}{2^j}\left(\underbrace{0, \ldots, 0}_{d\text{times}}, 1, 2, \ldots, 2^j - 1, \underbrace{2^j, \ldots, 2^j}_{d\text{times}}\right) \tag{12}$$

Here $j \in \mathrm{Z}$ is the level of detail and $d - 1 \in \mathrm{N}_0$ is the polynomial degree. In Eq. (11), the index $k = 1, \ldots, 2^j + d$ is used as a "shift" parameter, and $\phi_k^0(x)$ denotes the set of B-spline scaling functions of level zero. Splines of higher degrees $d > 1$ can be obtained using the recursion

$$\phi_k^r(x) := \frac{x - x_k}{x_{k+r} - x_k}\phi_k^{r-1}(x) + \frac{x_{k+r+1} - x}{x_{k+r+1} - x_{k+1}}\phi_{k+1}^{r-1}(x) \tag{13}$$

where $r = 1, \ldots, d-1$ refers to the recursion number. Equation (13) interpolates between the $r + 1$ knots neighboring knot x_k. The multiplication of $\phi^{r-1}(x)$ with x increases the polynomial degree by 1. Note that the fractions in Eq. (13) are replaced by zero when their denominators are zero.

The knot values of the scaling functions of a certain level space j are stored in the matrix $\Phi_j = (\phi_{j,i,k}) = (\phi_{j,k}(x_i))$, where each column represents the value of a scaling function for a certain location. Φ_j is a $m \times (2^j + d)$ matrix, where m represents the number of sampled data points and $2^j + d$ the number of scaling function values for the level space j. Accordingly, Φ_0 denotes the whole space of level zero, including all shifted versions of the scaling function in the spatial domain. It has to be pointed out that the scaling functions of a level space are not overall identical versions of each other. Due to multiple knots, given by the first d zero entries and the last d constant entries of the knot sequence (Eq. 12), the recursion scheme (Eq. 13) creates endpoint-interpolating B-splines. The non-uniformity of the scaling functions of level space $j = 2$ for degree $d = 2$ and $d = 4$ are shown in Fig. 1. Outside the unit interval [0; 1], the scaling functions are defined as $\phi_j^d(x) = 0$.

3 Filter bank for two-dimensional B-spline wavelets

The endpoint interpolating scaling functions can also be refined, since level spaces form nested subspaces, and consequently for all levels $j = 1, 2, \ldots, J$ there must exist a matrix $\mathbf{P}_j$ such that the two-scale relation

$$\Phi_{j-1} = \Phi_j \mathbf{P}_j \tag{14}$$

holds. The matrix $\mathbf{P}_j$ is of size $(2^j + d - 1) \times (2^{j-1} + d - 1)$. Each column in $\mathbf{P}_j$ contains the coefficients that belong to one scaling function. The wavelet spaces are also subspaces of higher-level spaces, thus a $(2^j + d - 1) \times (2^{j-1})$ matrix

$\mathbf{Q}_j$ exists that generates the wavelet matrix Ψ_{j-1} through

$$\Psi_{j-1} = \Phi_j \mathbf{Q}_j \tag{15}$$

The mathematical background for the generation of the **P** and **Q** matrices can be found in Quak and Weyrich (1994). Their approach forms a semi-orthogonal B-spline wavelet basis, fulfilling the condition

$$\langle \phi_{j,k}, \psi_{j,l} \rangle = 0 \quad \text{for all } j, k, l, \tag{16}$$

which means that the wavelet functions are orthogonal to the scaling functions, but not to each other within one level. With the conditions in Eqs. (14) to (16) and a given set of scaling functions, there are still a large number of possible **Q** matrices. Out of these, Stollnitz et al. (1996) constructed the **Q** matrix with a minimum number of non-zero entries, leading us to compactly supported B-spline wavelets.

Using the tensor product for level spaces, the two-dimensional basis functions read:

$$\begin{aligned}
&\phi(x, y) := \phi(x) \cdot \phi(y) \text{ scaling function} \\
&\psi_1(x, y) := \phi(x) \cdot \psi(y) \text{ vertical} \\
&\psi_2(x, y) := \psi(x) \cdot \phi(y) \text{ horizontal} \\
&\psi_3(x, y) := \psi(x) \cdot \psi(y) \text{ diagonal wavelet function}
\end{aligned} \tag{17}$$

where $\phi(x)$ and $\phi(y)$ are the one-dimensional scaling functions for the x- and y-direction on a two-dimensional manifold (such as the plane). The three types of two-dimensional wavelet functions are of different shape, enabling the absorption of vertical, horizontal or diagonal patterns in the spatially distributed data.

Let us assume $\mathbf{t} \in \mathrm{R}^2$ is a position vector. With the wavelet decomposition, the observed signal $y(\mathbf{t})$ is decomposed into a smoothed signal and a sum of different signals at various levels of detail as follows:

$$y(\mathbf{t}) - e(\mathbf{t}) = \sum_{k \in^2} c_{j_{\min},k} \tilde{\phi}_{j_{\min},k}(\mathbf{t}) + \sum_{j=j_{\min}}^{J} \sum_{\eta=1}^{3} \sum_{k \in^2} d_{j,k}^{\eta} \tilde{\psi}_{j,k}^{\eta}(\mathbf{t}) \tag{18}$$

The observational error of $y(\mathbf{t})$ is denoted by $e(\mathbf{t})$, which will be a set of zeros if the number of coefficients is equal to the number of gridded data points given. The adjustment of Eq. (18) leads to the determination of the unknown scaling function coefficients $c_{j_{\min},k}$ as well as the wavelet coefficients $d_{j,k}^{\eta}$. The different levels of detail are denoted by the index j. Wavelet coefficients with a larger j represent higher detail levels expressing the high-frequency part. The index η sums up the three directional components introduced in Eq. (17) and the index $k = [k_1, k_2]$ shifts the wavelets to different locations on the manifold.

Strictly speaking, the reconstruction of the signal requires the use of the dual scaling and wavelet functions, denoted by a tilde symbol. The construction of the duals can be found in Quak and Weyrich (1994). However, using the synthesis scheme (Eq. 20) does not involve the dual functions. In fact, the calculation of the coefficients can be carried out in a simple and computationally efficient way using a filter-bank procedure for decomposition. A step of this recursive process is given by

$$\left[\mathbf{P}_j \mathbf{Q}_j\right]^{-1} \mathbf{C}_j \left(\left[\mathbf{P}_j \mathbf{Q}_j\right]^{-1}\right)^{\mathrm{T}} = \begin{bmatrix} \mathbf{C}_{j-1} & \mathbf{D}_{j-1}^{1} \\ \mathbf{D}_{j-1}^{2} & \mathbf{D}_{j-1}^{3} \end{bmatrix} \tag{19}$$

Starting from the scaling coefficients of the highest-level $\mathbf{C}_J$, all scaling and wavelet coefficients of lower levels can be derived. The scaling coefficients are conveniently stored in form of a $(2^j + d - 1) \times (2^j + d - 1)$ matrix $\mathbf{C}_j$ according to their spatial position, whereas the three sub-matrices $\mathbf{D}_{j-1}^{\eta}$ contain the wavelet coefficients of the three directional components. The matrices **P** and **Q** can be seen here as refinement matrices and do not depend on the data. The synthesis of all detail signals is done with the inverse filter-bank procedure

$$\mathbf{C}_j = \left[\mathbf{P}_j \mathbf{Q}_j\right] \begin{bmatrix} \mathbf{C}_{j-1} & \mathbf{D}_{j-1}^{1} \\ \mathbf{D}_{j-1}^{2} & \mathbf{D}_{j-1}^{3} \end{bmatrix} \left[\mathbf{P}_j \mathbf{Q}_j\right]^{\mathbf{T}} \tag{20}$$

where the scaling coefficients of the highest level can be obtained in the last step. If the data are on a rectangle rather than on a square, the highest levels J_x and J_y for the data in x- and y-directions differ from each other. In order to maintain clarity, this is not considered here.

4 Tensor product for two-dimensional data

When implementing a filter-bank procedure as described in Sect. 3, the first step is to adjust the system of linear equations $\mathbf{y} - \mathbf{e} = \Phi\ \mathbf{c}_J$ in order to estimate the state vector for unknown coefficients of the highest level J from a given observation vector **y**. Here, the coefficients $\mathbf{c}_J$ form a vector $\mathbf{c}_J = \mathrm{vec}(\mathbf{C}_J)$, where the vec-operator writes the columns of $\mathbf{C}_J$, one underneath the other. With the covariance matrix of observations $D(\mathbf{y}) = \sigma^2 \mathbf{I}$, the least-squares solution is

$$\hat{\mathbf{c}}_j = (\Phi^{\mathrm{T}} \Phi)^{-1} \Phi^{\mathrm{T}} \mathbf{y} \tag{21}$$

The matrix Φ is a large $n\times$, m matrix, where n is the number of observations and $m = (2^J + d - 1)^2$ the number of coefficients (d again denotes the polynomial degree). The use of Eq. (21) allows scattered data to be handled, but only with a large storage and calculation effort. In order to handle large two-dimensional data efficiently on a raster, the matrix Φ can be split up into the two one-dimensional scaling matrices Φ_x and Φ_y for the x- and y-directions, respectively

$$\Phi = \Phi_y \otimes \Phi_x \tag{22}$$

where $\otimes$ is the Kronecker product of matrices. For the definition and some important properties of the Kronecker product see, e.g., Koch (1999, p 19, 41). Substituting $\Phi = \Phi_y \otimes \Phi_x$ in Eq. (21) we obtain

$$\hat{\mathbf{c}}_J = [(\Phi_y \otimes \Phi_x)^{\mathrm{T}} (\Phi_y \otimes \Phi_x)] (\Phi_y \otimes \Phi_x)^{\mathrm{T}} \mathbf{y} \tag{23}$$

and, after applying the Kronecker product laws (*ibid.*),

$$\hat{\mathbf{C}}_J = (\Phi_x^{\mathrm{T}} \Phi_x)^{-1} \Phi_x^{\mathrm{T}} \mathbf{Y} \Phi_y (\Phi_y^{\mathrm{T}} \Phi_y)^{-1} \tag{24}$$

with $\mathbf{y} = \mathrm{vec}(\mathbf{Y})$. The matrix **Y** represents equidistantly spaced data points (in terms of the chosen parameterization). In order to demonstrate the computational benefit of Eq. (24), assume

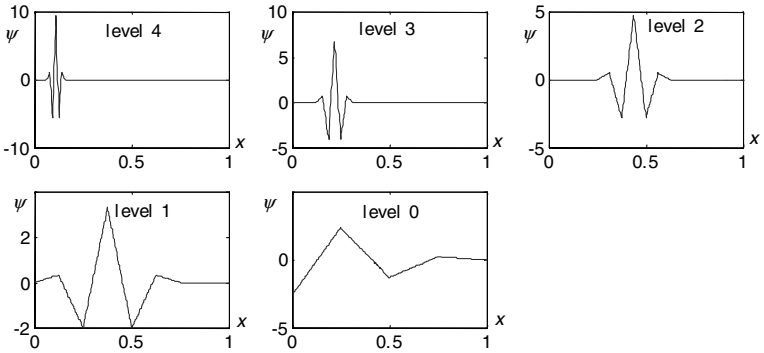

Fig. 2 One-dimensional linear B-spline wavelets of detail levels 0–4. Out of all wavelets within one level, only one version with unbounded domain is displayed here

a 1024×1024 dataset $\mathbf{Y}$. Using Eq. (24), the calculation of $\Phi_x^{\mathrm{T}}\Phi_x$ takes about 10^9 multiplications, which is much less than the 10^{18} multiplications for $\Phi^{\mathrm{T}}\Phi$ in Eq. (21).

Using the Kronecker product approach, one can efficiently view the directional detail signals $\mathbf{G}$ by

$$\begin{aligned} &\mathbf{G}_{j,1}\Phi_{x,j}\mathbf{D}_j^1\Psi_{y,j}^{\mathrm{T}} \\ &\mathbf{G}_{j,2}\Psi_{x,j}\mathbf{D}_j^2\Psi_{y,j}^{\mathrm{T}} \\ &\mathbf{G}_{j,3}\Psi_{x,j}\mathbf{D}_j^3\Psi_{y,j}^{\mathrm{T}} \end{aligned} \tag{25}$$

where the wavelet coefficient matrices $\mathbf{D}$ are determined by Eq. (19). The complete signal of detail level j is given by $\mathbf{G}_j = \mathbf{G}_{j,1} + \mathbf{G}_{j,2} + \mathbf{G}_{j,3}$, and the sum $\mathbf{G}_j$ over all $j = 1, 2, ..., J$ reconstructs the data.

The construction of spherical pseudo-wavelets (Schaffrin et al. 2003) can be achieved, e.g., by a Mercator projection from a spherical patch in longitude λ and isometric latitude q, defined by

$$q = \mathrm{In}\,\tan(\pi/4 + \varphi/2) \tag{26}$$

where ϕ is the latitude. Since the wavelet representation is defined on the standard (planar) quadrangle $-1 \le x \le +1$ and $-1 \le y \le +1$, the data positions are normalized by

$$x = \frac{2\lambda - \lambda_{\max} - \lambda_{\min}}{\lambda_{\max} - \lambda_{\min}} \quad \text{and} \quad y = \frac{2q - q_{\max} - q_{\min}}{q_{\max} - q_{\min}} \tag{27}$$

where $\lambda_{\min}$, $q_{\min}$ and $\lambda_{\max}$, $q_{\max}$ are the boundaries of a patch on the sphere. The wavelet analysis is then performed in a quasi-plane for each patch separately. With the inverse relation of Eq. (26), namely

$$\varphi = 2\ \mathrm{arc}\,\tan(\mathrm{e}^q)\pi/2 \tag{28}$$

the wavelet basis is transferred back onto the sphere, where the exact wavelet properties will be lost. However, this does not narrow its applicability as a model function. The mathematical background can be found in Schaffrin et al. (2003), including techniques for a decomposition of the sphere by an Igloo data-structuring approach.

5 Space and frequency localization

Wavelets localize both in the space and frequency domains. However, due to the Heisenberg uncertainty relation, it is not possible to exactly determine one frequency at a specific position. The variations in space and frequency for a function are measured using the Heisenberg Box, whose optimal size is 2.0 when applied to the Gauss function. For the linear B-spline wavelets, the box size becomes 3.88, which is fairly good. The cubic B-spline wavelets have an almost optimal box size of 2.02, allowing an excellent analysis of data in terms of location and frequency content.

Every level of detail represents a certain frequency band; thus, the values of the wavelet coefficients will directly reflect the frequency content at different locations. Some examples of the one-dimensional linear B-spline wavelets are illustrated in Fig. 2. The signal of different detail levels based on linear B-spline wavelets displaying TEC in the Pacific are shown in Fig. 3. Furthermore, every level of detail can be split up into components along the diagonal, horizontal and vertical axes, allowing further investigations of directional structures in the data. Figure 4 shows an analysis of a detail signal based on linear B-splines.

6 Temporal and spatial representation of TEC

Here we study the representation and modeling of variations of TEC over Japan observed by GEONET using the above-mentioned approaches. The accuracy of GPS is affected by variations in the dispersive medium between the transmitter onboard the satellites and the ground (signal) receivers. On the other hand, this effect can be used to derive the TEC of the ionosphere, measured in units of 10^{16} electrons/m^2 (TECU), from the Earth's surface (receiver) to the GPS satellite orbiting at ~20,000 km altitude in space. The time delay or phase advance of the GPS signal is proportional to ionospheric TEC along the path of the electromagnetic wave, and it is inversely proportional to the square of the frequency. Using these relations, the first-order ionospheric TEC is estimated by combining L1 and L2 pseudo-range or phase measurements obtained by a dual-frequency GPS receiver.

With GEONET continually operating over Japan, pixel maps of daily relative TEC variations are estimated every 30 s, corresponding to the sampling period of GEONET GPS receivers. The precision of the relative TEC is better than 0.1 TECU with an equidistant spatial distribution of

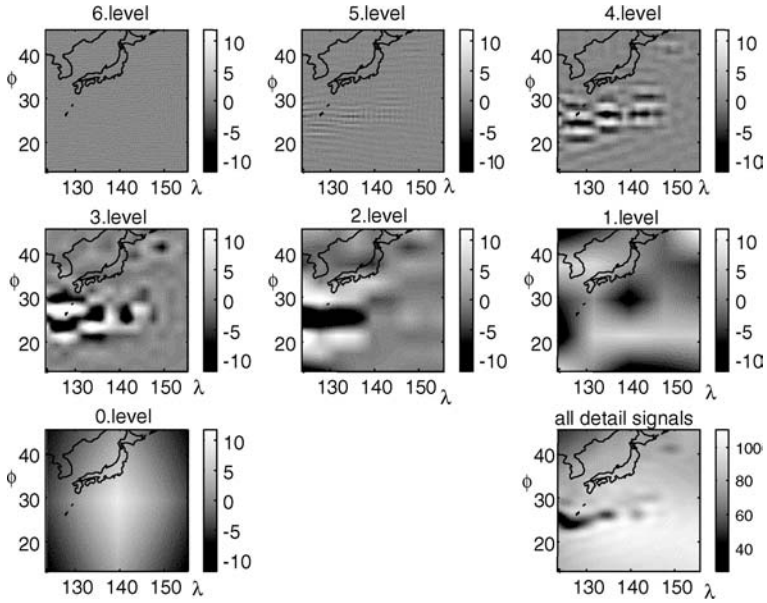

Fig. 3 Different detail signals of TEC values over a 32° × 32° patch in the Pacific Ocean. Most of the energy can be found in the detail levels 2 and 3. The *lower right image* shows the complete signal as the sum of all detail levels. TEC values are in TECU (10^{16} /m^2)

0.15° × 0.15° (Saito et al. 1998), and is processed at the University of Kyoto. Despite the high-resolution and -precision, the following two basic problems arise: (1) instrumental biases between satellite and receiver in the pseudo-ranges and (2) data gaps caused by unevenly distributed ground stations, irregular satellite passes, and data outages (e.g., over the ocean).

Otsuka et al. (2002) developed an algorithm to solve the first problem, obtaining an accuracy of absolute TEC of 1–3 TECU, depending on the geomagnetic latitude. The so-obtained absolute TEC along the path between satellite and receiver is then projected onto the zenith direction using suitable mapping functions.

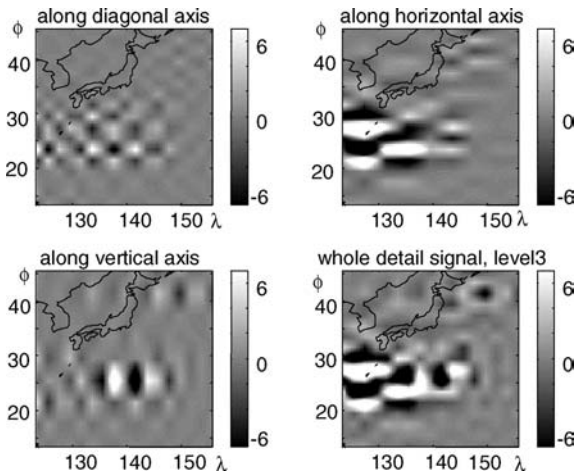

Fig. 4 Detail signals of TEC values along the diagonal, horizontal and vertical axes over a 32° × 32° patch in the Pacific Ocean for detail level 3. The *lower right image* represents the complete detail signal of level 3. TEC values are in TECU (10^{16} /m^2)

The second problem is mitigated to a certain extent by using a wider-spaced grid of 0.25° × 0.25° and a sampling rate of 10 min. This choice is based on experience, since there is no significant improvement when using finer temporal sampling. The selection of a 0.25°-grid is a compromise between preserving detailed information and the need to fill data gaps. The GEONET maps are compared with the Center for Orbit Determination in Europe (CODE) global ionosphere map (GIM) computed using a much coarser global GPS network (Schaer et al. 1995) and merged with the GIM for corresponding epochs (Ping et al. 2002, 2003). The average difference between the CODE GIM and GEONET TEC over Japan is about 3–5 TECU depending on the number of International GPS Service (IGS) receivers used in the estimation of the GIM.

After pre-processing the data as mentioned above, the gridded TEC time series with equidistant spatial distribution serves as input for the following analysis. For areas where there are no ionosphere observations, we fill in the data gaps using the GIM model with a coarser resolution of 12° × 12° and with 2-h sampling. Hence, it is not possible to derive high-frequency signals for these areas, and the accuracy and resolution of the gridded TEC time series are non-uniform. In this study, we choose to process equidistant spatial and temporal TEC data using B-spline wavelets as a demonstration of the efficiency of the proposed technique to "model" this gridded time series.

The (2+1)-dimensional (latitude, longitude and time) array of TEC values yt) is used to model the B-spline wavelets in space (as described in Sects. 3 and 4), and standard cubic splines are used for interpolation in time. The natural cubic spline was chosen, as it is the smoothest of all possible interpolating curves in the sense that it minimizes the integral of the square of the second derivative. Altogether a

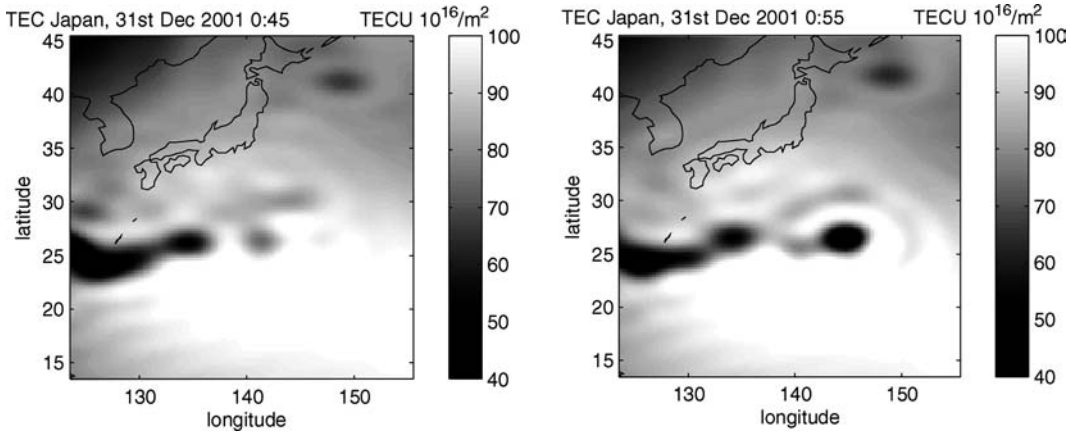

Fig. 5 TEC values in TECU (10^{16}/m^2) for 123.5–155.5° longitude and 13.5–45.5° latitude for 31st Dec 2001 at 0:45 AM (*left*) and 0:55 AM (*right*) represented by linear B-spline wavelets consisting of detail levels 0–7

Table 1 Different compression values, resulting root mean squared deviations and maximal deviations $\delta_{\max}$

Compression (%)	No. of remaining coefficients	rms deviation [TECU]	$\lvert\delta_{\max}\rvert$ [TECU]
0.0	16,641	0	0
75.0	4,161	0.024	0.10
90.0	1,665	0.098	0.55
95.0	833	0.202	1.29
99.0	167	0.937	6.86

continuous (2+1)-dimensional model of TEC is obtained with the number of continuous derivatives depending on the polynomial degree d of the basis functions. Thus, the wavelet approach not only allows us to evaluate the model at arbitrary points, but also to determine the change of TEC in time (∂TEC/$\partial\, t$).

Figure 5 shows two points in time of the wavelet representation for TEC over Japan with a time step of 10 min. With the data being the same size as the set of coefficients, the model does not deviate at the locations of the observations, besides small computer rounding errors. Each representation for one point in time is a synthesis of $(2^7+1)^2 = 16{,}641$ coefficients. In Fig. 6, the result of a cubic spline interpolation between the observed times at 0:35, 0:45, 0:55 and 1:05 UTC is shown for 0:50 UTC. The model allows the derivation of TEC values for any point in time and space within the given observational frame. Storing the model for one day of data needs a comparatively small number of $144\cdot(2^7+1)^2$ (ca. 2.4 Mio) coefficients.

When plotting the magnitude of the coefficients, the histogram may have a high peak for small values. Therefore, a large number of coefficients can be neglected via a thresholding process without any major loss of information. This is obviously the case for wavelet coefficients resulting from TEC, as shown in Fig. 7. Such data compression leads to relatively small root mean square deviations for high compression factors. An application of B-spline compression was carried out in Schaffrin et al. (2003). The result of compression of TEC values for the abovementioned patch in the Pacific Ocean is shown in Table 1. Neglecting 90% of the wavelet coefficients leads to a root mean squared devi-

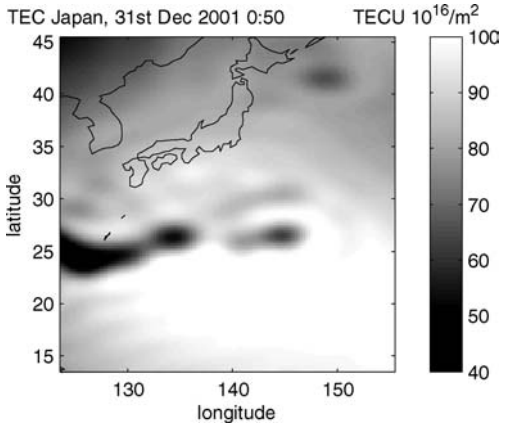

Fig. 6 TEC values in TECU (10^{16}/m^2) interpolated with cubic splines for 31st Dec 2001 for 0:50 AM, based on the observations at 0:35 AM, 0:45 AM, 0:55 AM and 1:05 AM UTC

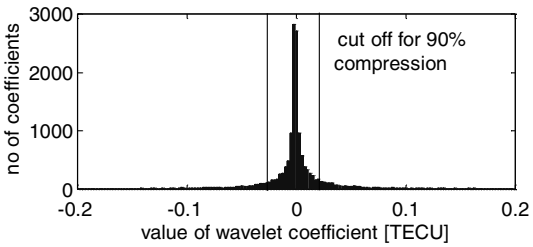

Fig. 7 Distribution of wavelet coefficients according to their magnitude. The coefficients are derived from TEC data 31st Dec 2001 for 0:45 over the Japan Islands. For 90% compression, wavelet coefficients less then 0.021 TECU are set to zero

ation from the uncompressed signal of ± 0.098 TECU. This result varies slightly with the roughness or smoothness of the data.

7 Discussion and conclusions

For the representation of the ionospheric TEC distribution and its variation, the spherical harmonic method still plays an important role in global or regional studies. The Stokes coefficients of the spherical harmonics can be estimated by using surface integration even for unevenly gridded TEC. The spatial and time interpolation can be obtained with sufficient accuracy for medium- or low-frequency components. However, in order to model a spherical field with high spatial resolution and precision by using spherical harmonic functions, Stokes coefficients of commensurate high degree and order are needed. The total number of coefficients may be comparable with that of the corresponding gridded observations themselves. For rapidly (temporal and spatial) varying datasets like the ionospheric TEC, it is inefficient and inaccurate to use spherical harmonics, especially when multi-resolution representation is desirable.

For a representation of the Earth's ionosphere, the two-dimensional B-spline wavelets, combined with a cubic spline interpolation in time, have been demonstrated to be capable of efficient representation or modeling of a regional (2+1)-dimensional TEC dataset. The property of compact support and the usage of tensor products allow a computationally efficient wavelet representation. While the wavelet representation is carried out on the plane, the exact wavelet properties are lost when transferring the model back to the sphere. Nevertheless, the advantages of the wavelet model have been maintained: fast access to evaluate the model at arbitrary points, while maintaining their variation-diminishing and continuity properties between the observational points. Applications in terms of data analysis and multi-resolution representations further illustrate the usefulness of the model. The wavelet approach also allows data compression and decompression for huge datasets such as GIMs.

For future work, we are considering an updated algorithm to directly model unevenly distributed regional spatial and temporal TEC observations by using B-spline wavelets, to better preserve signals and achieve multi-resolution properties of the resulting synthesis. The algorithm may have to include adjustment techniques and is computationally more intensive. Another related aim is to develop a (3+1)-dimensional TEC model combining space data with distinct accuracy and distributions following the suggestions of Potts et al. (2003).

Acknowledgements We thank Geographical Survey Institute of Japan for providing the GEONET GPS data and Drs. A. Saito and Y. Otsuka for their help on GEONET TEC data analysis. The GIM data is from the Center for Orbit Determination in Europe (CODE) and computed from International GPS Service (IGS) data. J. Ping and K. Heki acknowledge the Japan Society for the Promotion of Science (JSPS) for supporting this study. R. Mautz acknowledges the support of a Feodor-Lynen scholarship from the Alexander-von-Humboldt Foundation (Germany), and the Laboratory for Space Geodesy and Remote Sensing at the Ohio State University (USA). C. Shum and L. Potts are is supported by grants from NGA's University Research Initiative (NURI) program, and from the National Science Foundation's Aeronomy program (ATM-0418844).

References

Chui CK, Wang JZ (1992) On compactly supported spline wavelets and a duality principle. Trans Am Math Soc 330(2):903–915

Chui CK, Quak E (1992) Wavelets on a bounded interval. In: Braess D, Schumaker L (eds) Numerical methods in approximation theory, Vol 9. Birkhäuser, Basel Boston Berlin, pp 53–77

Freeden W (1999) Multiscale modelling of spaceborne geodata. Teubner, Stuttgart

Koch K (1999) Parameter estimation and hypothesis testing in linear models. Springer, Berlin Heidelberg New York

Lyche T, Schumaker L (2000) A multiresolution tensor spline method for fitting functions on the sphere. SIAM J Sci Comput 22(2):724–746. DOI 10.1137/S1064827598344388

Mautz R, Schaffrin B, Schmidt M, Shum CK (2002) Representation of spatial functions in geodesy using B-spline wavelets with compact support. In: Presented at the Weikko A. Heiskanen symposium in geodesy, Ohio State University, Columbus

Otsuka Y, Ogawa T, Saito A, Tsugawa T, Fukao S, Miyazaki S (2002) A new technique for mapping of total electron content using GPS network in Japan. Earth Planets Space 54(1):63–70

Ping J, Kono Y, Matsumoto K, Otsuka Y, Saito A, Shum CK, Heki K, Kawano N (2002) Regional ionosphere map over Japanese Islands. Earth Planets Space 54(12):el3–el6

Ping J, Kono Y, Matsumoto K, Otsuka Y, Saito A, Sekido M, Shum CK, Heki K, Kawano N (2003) Developing and upgrading a regional ionosphere map over Japan islands based on GEONET observation. In: Proceedings of the International symposium on GPS/GNSS, Tokyo, November

Potts L, Schmidt M, Shum CK, Ge S (2003) Wavelet based regional multi-resolution TEC model. (abstract), European Geophysical Society–American Geophysical Union–European Union of Geosciences Joint Assembly, Nice, April

Quak E, Weyrich N (1994) Decomposition and reconstruction algorithms for spline wavelets on a bounded interval. Appl Comput Harmon Anal 1(3):217–231

Saito A, Fukao S, Miyazaki S (1998) High resolution mapping of TEC perturbations with the GSI GPS network over Japan. Geophys Res Lett 25(16):3079–3082

Salamonowicz PH (2001) A wavelet-based gravity model with an application to the evaluation of Stokes' integral. In: Sideris MG (ed) Gravity, geoid and geodynamics 2000. Springer, Berlin Heidelberg New York, pp 85–90

Schaffrin B, Mautz R, Shum CK, Tseng H (2003) Towards a spherical pseudo-wavelet basis for geodetic applications. Comput Aided Civ Inf 18(5):369–378. DOI 10.1111/1467–8667.t01–1-00314

Schmidt M (2001) Basic principles of the wavelet analysis with applications to geodesy (in German), Habilitation thesis, Shaker. Aachen

Schaer S, Beutler G, Mervart L, Rothacher M, Wild U (1995) Global and regional ionosphere models using the gps double difference phase observable. In: Gendt G, Dick G (eds) Proceedings of the IGS workshop on special topics on new directions, potsdam, pp 77–92

Stollnitz E, DeRose T, Salesin D (1996) Wavelets for computer graphics. Kaufmann, San Francisco

Wilson BD, Mannucci AJ, Edwards CD (1995) Subdaily northern hemisphere ionospheric maps using an extensive network of GPS receivers. Radio Sci 30:639–648